AD-A175 741 THE INITIAL GIANT UMBRELLA CLOUD OF THE MAY 18 1980 1/1
EXPLOSIVE ERUPTION OF..(U) AEROSPACE CORP EL SEGUNDO CA
SPACE SCIENCES LAB R S SPARKS ET AL. 30 SEP 86
UNCLASSIFIED TR-0086(6940-03)-1 SD-TR-86-62 F/G 4/2 NL

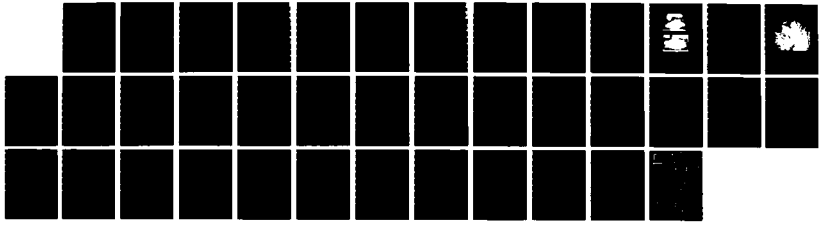

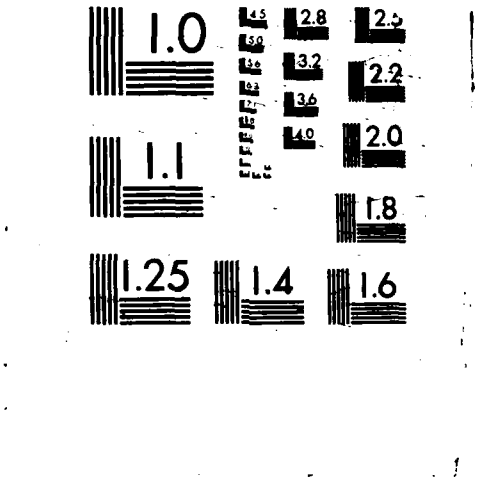
1.0
1.1
1.25
1.4
1.6
1.8
2.0
2.2
2.5
2.8
3.2
3.6
4.0
4.5
5.0

REPORT SD-TR-86-62

(12)

The Initial Giant Umbrella Cloud of the May 18, 1980 Explosive Eruption of Mount St. Helens

R. S. J. SPARKS
Department of Earth Sciences
University of Cambridge
Cambridge CB2 3EQ, England

J. G. MOORE
U.S. Geological Survey
345 Middlefield Road
Menlo Park, CA 94025

and

C. J. RICE
Space Sciences Laboratory
The Aerospace Corporation
El Segundo, CA 90245

30 September 1986

Prepared for
SPACE DIVISION
AIR FORCE SYSTEMS COMMAND
Los Angeles Air Force Station
P.O. Box 92960, Worldway Postal Center
Los Angeles, CA 90009-2960

This report was submitted by The Aerospace Corporation, El Segundo, CA 90245, under Contract No. F04701-85-C-0086 with the Space Division, P.O. Box 92960, Worldway Postal Center, Los Angeles, CA 90009-2960. It was reviewed and approved for The Aerospace Corporation by H. R. Rugge, Director, Space Sciences Laboratory.

Capt Kevin O'Brien/YNCS was the project officer for the Mission-Oriented Investigation and Experimentation (MOIE) Program.

This report has been reviewed by the Public Affairs Office (PAS) and is releasable to the National Technical Information Service (NTIS). At NTIS, it will be available to the general public, including foreign nationals.

This technical report has been reviewed and is approved for publication. Publication of this report does not constitute Air Force approval of the report's findings or conclusions. It is published only for the exchange and stimulation of ideas.

Kevin O'Brien

KEVIN O'BRIEN, Capt, USAF
MOIE Project Officer
SD/YNCS

Joseph Hess

JOSEPH HESS, GM-15
Director, AFSTC West Coast Office
AFSTC/WCO OL-AB

UNCLASSIFIED

SECURITY CLASSIFICATION OF THIS PAGE *(When Data Entered)*

REPORT DOCUMENTATION PAGE

READ INSTRUCTIONS BEFORE COMPLETING FORM

1. REPORT NUMBER: SD-TR-86-62

2. GOVT ACCESSION NO.: A175 941

3. RECIPIENT'S CATALOG NUMBER:

4. TITLE *(and Subtitle)*: THE INITIAL GIANT UMBRELLA CLOUD OF THE MAY 18, 1980 EXPLOSIVE ERUPTION OF MOUNT ST. HELENS

5. TYPE OF REPORT & PERIOD COVERED:

6. PERFORMING ORG. REPORT NUMBER: TR-0086(6940-03)-1

7. AUTHOR(s): R. Stephen J. Sparks, James G. Moore, and Carl J. Rice

8. CONTRACT OR GRANT NUMBER(s): F04701-85-C-0086

9. PERFORMING ORGANIZATION NAME AND ADDRESS: The Aerospace Corporation, El Segundo, Calif. 90245

10. PROGRAM ELEMENT, PROJECT, TASK AREA & WORK UNIT NUMBERS:

11. CONTROLLING OFFICE NAME AND ADDRESS: Space Division, Los Angeles Air Force Station, Los Angeles, Calif. 90009-2960

12. REPORT DATE: 30 September 1986

13. NUMBER OF PAGES: 32

14. MONITORING AGENCY NAME & ADDRESS *(if different from Controlling Office)*:

15. SECURITY CLASS. *(of this report)*: Unclassified

15a. DECLASSIFICATION/DOWNGRADING SCHEDULE:

16. DISTRIBUTION STATEMENT *(of this Report)*

Approved for public release; distribution unlimited.

17. DISTRIBUTION STATEMENT *(of the abstract entered in Block 20, if different from Report)*

18. SUPPLEMENTARY NOTES

19. KEY WORDS *(Continue on reverse side if necessary and identify by block number)*

Mount St. Helens
Pyroclastic flow
Volcanic clouds
Volcanic eruption

20. ABSTRACT *(Continue on reverse side if necessary and identify by block number)*

The initial eruption column of May 18, 1980 reached nearly 30 km altitude and involved the release of 10^{17} joules of thermal energy into the atmosphere in only a few minutes. Ascent of the cloud resulted in forced intrusion of a giant mushroom cloud between altitudes of 10 and 20 km at radial horizontal velocities initially in excess of 50 m/s. The mushroom cloud expanded 15 km upwind, forming a stagnation point where the radial expansion velocity and wind velocity were equal. The cloud was initiated when the

DD FORM 1473 (FACSIMILE)

UNCLASSIFIED

SECURITY CLASSIFICATION OF THIS PAGE *(When Data Entered)*

19. KEY WORDS *(Continued)*

20. ABSTRACT *(Continued)*

pyroclastic blast flow became buoyant by mixing and heating surrounding air. Observations indicate that much of the flow, covering an area of 600 km^2, became buoyant within a time-span of 1.5 min and abruptly ascended to form the giant cloud. Calculations are presented for the amount of air that needs to be entrained into the flow to make it buoyant. Assuming an initial temperature of 450°C and a magmatic origin for the explosion, these calculations indicate that the flow became buoyant when its temperature was approximately 150°C and the flow consisted of a mixture of 3.25×10^{11} kg of pyroclasts and 5.0×10^{11} kg of air. If sedimentation is considered, these figures reduce to 1.1×10^{11} kg of pyroclasts and 1.0×10^{11} kg of air.

PREFACE

R. S. J. S. is supported by the B. P. Venture Research Unit. J. S. Turner and S. N. Carey are thanked for useful discussions. Reviews of an earlier version of this work by Sue Kieffer and Chris Newhall were of considerable help. Permission to reproduce the photo-mosaic in Fig. 1a was given by Rocky Kolberg and James Kolberg and is greatly appreciated. Permission to publish the paper was granted by the U.S. Air Force and the U.S. Geological Survey.

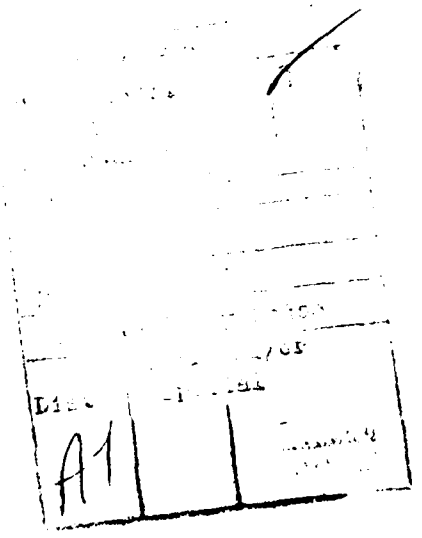

CONTENTS

FIGURES

TABLES

I. INTRODUCTION

The initial paroxysmal explosive eruption of Mount St. Helens on May 18, 1980 involved a complicated sequence of landslides, vertical explosions and a devastating horizontal blast, or pyroclastic flow. All these events took place within a few minutes and were immediately followed by the rapid ascent of an enormous eruption cloud that reached a height of nearly 30 km within 20 min. Data from military satellites allow the detailed behavior of this eruption column to be studied. This report presents these data, considers how the giant cloud relates to the initial events of the eruption, and interprets the data in terms of theoretical models of atmospheric convection. The most significant new observation is that the plume spread laterally at spectacular rates, forming a giant umbrella cloud. The umbrella cloud spread 15 km upwind. The implications of this behavior for understanding large-magnitude explosive eruptions are discussed.

II. OBSERVATIONS

The magnitude 5+ earthquake that occurred at Mount St. Helens at 15:32.2 UT on 18 May 1980 was immediately followed by landslide failure of the north flank and summit region of the volcano. Military and weather satellite data, together with ground photography, have enabled detailed documentation of the events in the first few minutes of the eruption as described by Rice (1981) and Moore and Rice (1984). Explosions were first observed at 15:32.7 from the summit region and from the moving landslide that fed a directed blast flow to the north. There is currently a controversy over whether the directed blast should be described as a surge or pyroclastic flow (Hobblitt and Miller, 1984; Walker and McBroome, 1983, 1984; Waitt, 1984). For simplicity we will refer to the phenomenon as a blast flow. The blast flow moved at more than 90 m/s, overtaking the avalanche at 15:33.8 UT. The blast flow reached its furthest point between 15:36 and 15:37, covering an area of over 600 km^2. At about this time a huge convecting column was observed to rise. In about ten minutes the cloud grew to form a giant mushroom-shaped cloud (Figs. 1 and 3) with a stalk diameter of over 20 km, a height of 25 km, and a mushroom cap of 70 km diameter. There is good agreement between the width of the cloud (interpreted from satellite data) and the position of the outer edges (deduced from the ground photographs) (see Fig. 2).

At least four distinct vertically rising clouds can be distinguished in the first 15 min of the eruption; these are identified in Fig. 4, which records data on their variation of height with time. Cloud I represents a coalescence of material formed by several explosions that occurred as the landslide blocks moved away from the volcanic cone. Photographs from Mount Adams, 53 km east of Mount St. Helens (Fig. 10.3 in Moore and Rice, 1984), show that the major effects in this period involved the lateral spreading of the blast flow, but that vertical motion also occurred, with the apex of an inverted cone-shaped cloud rising above an area about 4 km north of the summit region. The rise of the apex of this expanding region is recorded as Cloud I and had a mean vertical velocity of 25 m/s.

(a)

(b)

Fig. 1. Photographic mosaics of giant cloud taken from (a) U.S. Forest Service (1981), and (b) Rocky Kolberg. Both views are from north-west of Mount St. Helens. Kolberg photograph taken at about 15:52 GMT. U.S. Forest Service photograph taken at about 15:54 GMT. Both clouds subtend a horizontal angle of about 90°, as shown in Fig. 2. Photograph in Fig. 1b assembled by James F. Kolberg, President of the Toledo Poster Company.

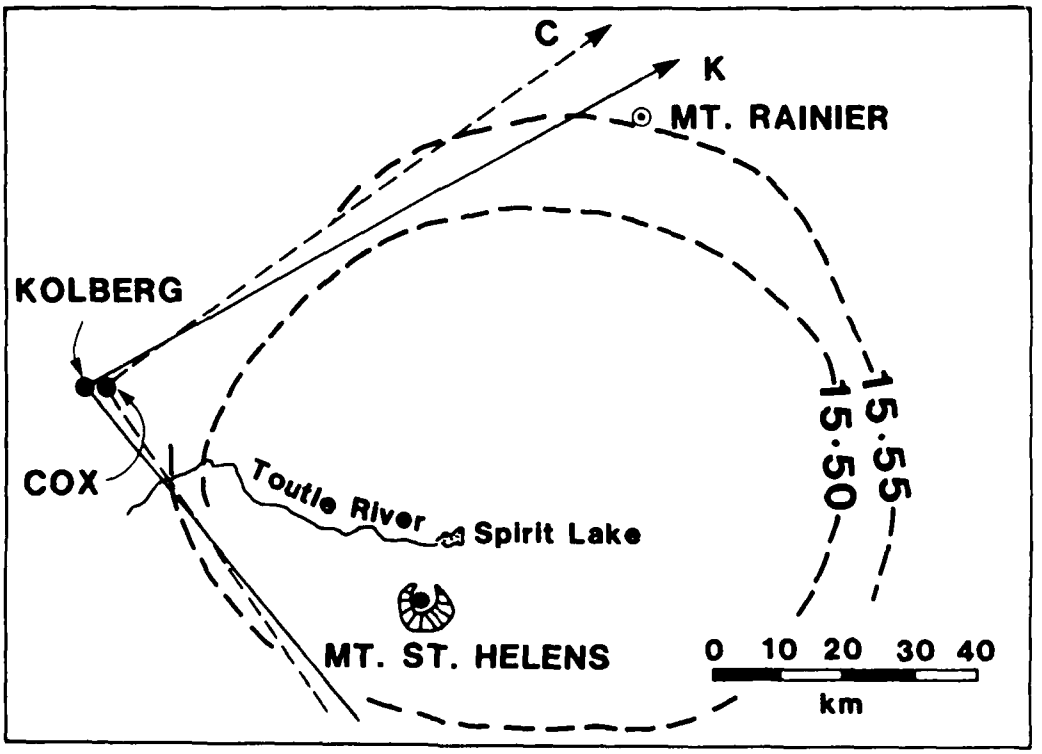

Fig. 2. Camera locations for the U.S. Forest Service and Kolberg photographic mosaics. Rays to the outer edge of the mushroom cap are shown for each photograph. The diameters of the cloud from interpretation of satellite images at 15:50 and 15:55 GMT are shown, which bracket the time when the photographs were taken (see Fig. 5).

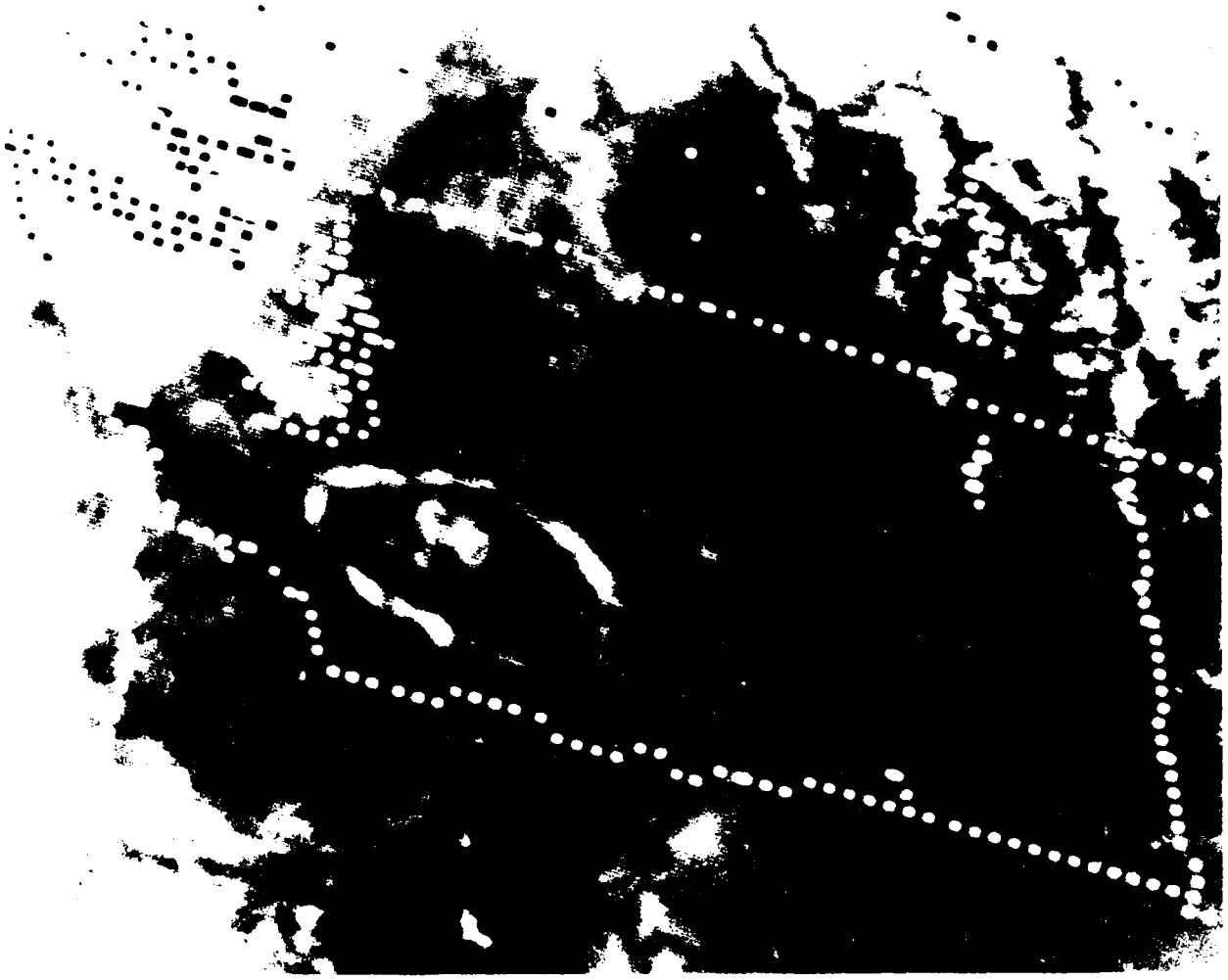

Fig. 3. GOES-West satellite image of giant cloud at 16:15 GMT. White dots give outline of Washington State. White fringe to cloud is interpreted to be a consequence of condensation.

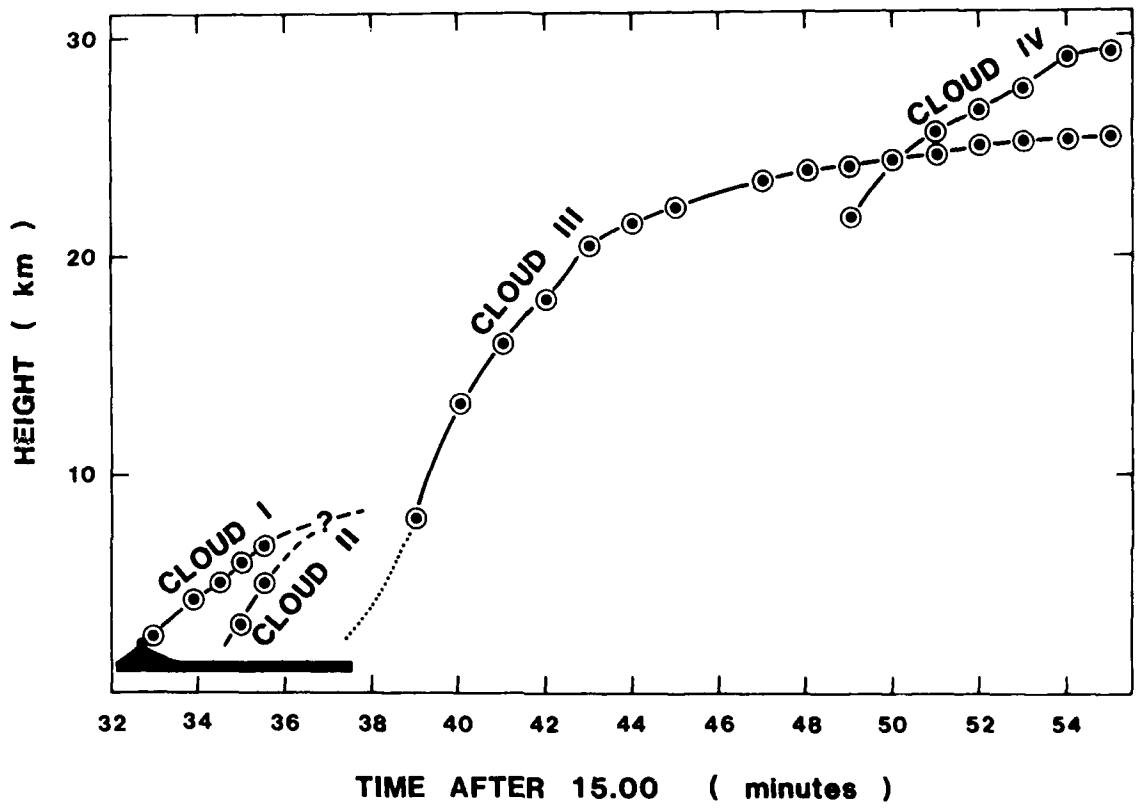

Fig. 4. Altitude of clouds above sea level versus GMT for initial stage of May 18 eruption. Four different clouds can be distinguished (see text). The horizontal bar represents the duration of the blast flow at ground level (2 km above sea level).

Photographic evidence (Moore and Rice, 1984) shows that a second cloud (Cloud II) began to rise rapidly from an area 12 to 13 km north of the summit above Spirit Lake and somewhat north of the Toutle River. Moore and Rice (1984) interpreted this cloud as the consequence of the second landslide, containing parts of the dacite cryptodome, moving into the Toutle River and Spirit Lake area. They envisage that the Cloud II explosions were produced when the landslide block slammed into the north wall of the Toutle River valley or shattered and interacted with water, triggering a large hydrovolcanic explosion. The only two data points on this cloud record a vertical velocity of 70 m/s (Fig. 4).

New information from U.S. military satellites has yielded unique data on the ascent and expansion of the main mushroom cloud. Figure 4 records the variation of height with time for the column. Two episodes of growth could be distinguished and are designated Clouds III and IV. Figure 5 shows the outline of the cloud as observed from Earth-orbiting satellites. The diagram shows cloud outlines at 5-min intervals and gives the first data on the radial expansion of a major eruption cloud. An example of the satellite view that can be obtained is shown in Fig. 3, which shows the giant cloud as observed from a GOES geostationary weather satellite at 16:15 GMT.

The initial vertical velocity of Cloud III is approximately 110 m/s and is clearly much more energetic than in the earlier explosions. Inspection of photographs and Fig. 4 indicates that the center of growth of the cloud was displaced to the north of Mount St. Helens, in the same region as the explosions that generated Cloud II. However, the data in Fig. 4 show that Cloud III cannot be related to the explosion that generated Cloud II, which evidently decelerated and could not have risen much above 10 km. There is a three-minute delay, apparent in the diagram, between the early explosions and the development of the major eruption column (Fig. 4). The blast cloud had reached its maximum extent between 15:36 and 15:37.5, at precisely the time the major cloud began its ascent. Descriptions of the blast (Moore and Sisson, 1981; Waitt, 1981) and abrupt termination of the zone of devastation (Kieffer, 1981) indicate that the blast cloud terminated lateral motion as it lifted off the ground and began to rise vertically. Data on flow velocities

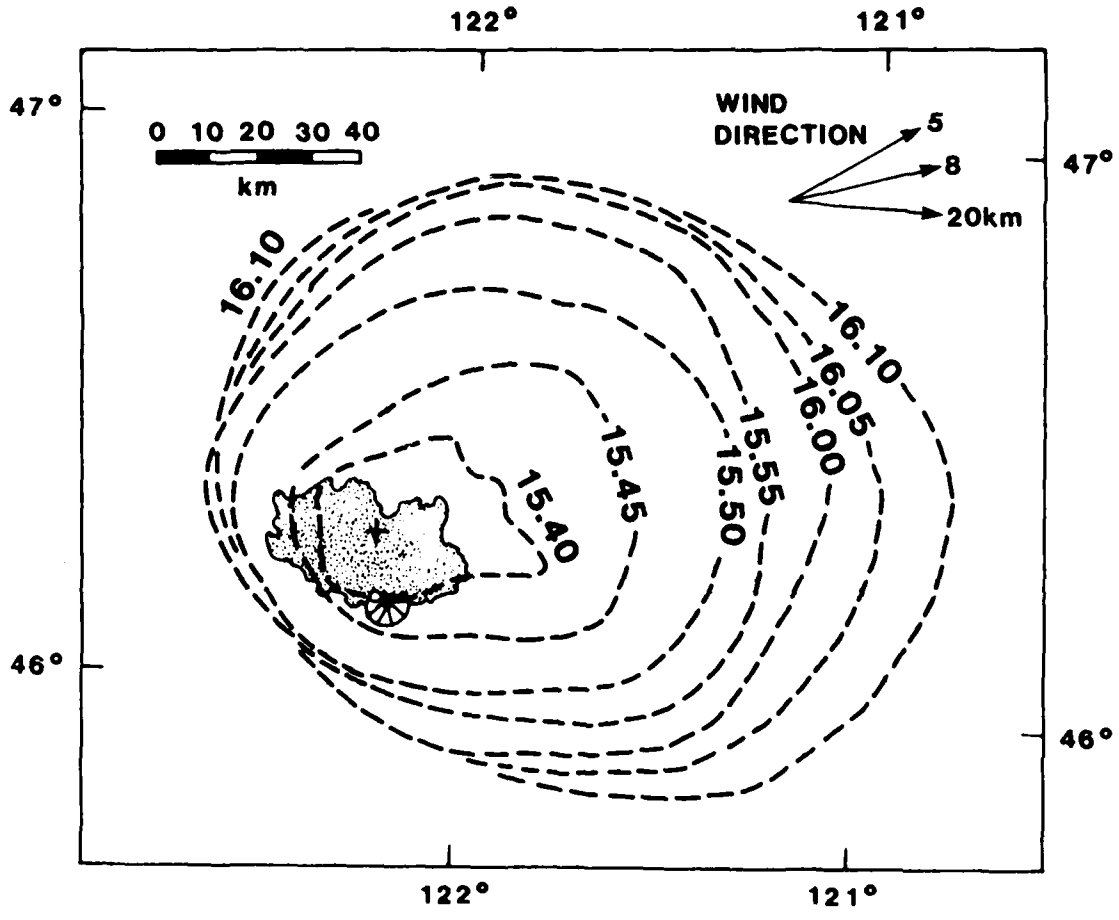

Fig. 5. Outline of the cloud at 5-min intervals as observed from geostationary satellites. Cross is estimate of initial center of cloud ascent. The stippled area shows extent of blast deposit. In the upper right hand corner the wind direction is shown as measured at Spokane on May 18 at elevations of 5, 8, and 20 km.

(Moore and Rice, 1984) show that the flow still had a velocity of about 100 m/s as it approached the distal edge, with little indication of any significant deceleration. The outer limit was thus determined not only by the flow slowing down but by the flow becoming buoyant. We conclude that the flow ascended to form a cloud when its density had become lower than the overlying atmosphere. We therefore interpret Cloud III to have formed by the buoyant ascent of the whole blast cloud over the entire 600-km^2 area. The main cloud was not in the strict sense generated by explosions, but by decompression of the flow, by mixing of air with the blast flow, and by sedimentation of pyroclasts.

The origin of Cloud IV is more problematic, since it must have originated several minutes after termination of lateral blast movement. At about 15:43 satellite sensors detected a pulse of new hot material rising vertically above the vent (Rice, 1981). Moore and Rice (1984) interpreted this as the onset of the plinian eruption, discharging predominantly high-temperature juvenile magma, which then continued for a further nine hours. Cloud IV extended the initial column to nearly 30 km altitude, but subsequent plinian activity only produced a column between 14 and 18 km high. The first stage of plinian activity, if manifested by Cloud IV, may have involved a much greater magma discharge rate than the subsequent plinian activity (approximately 10^5 m^3/s, as compared with 6000 m^3/s according to Sarna-Wojcicki et al., 1981). Alternatively, the initial plinian activity involved discharge into the giant cloud itself, which may have enabled the plinian column to rise to an unusually great height. Shortly after 16:00 the column height decreased dramatically to about 14 km.

The satellite views of the cloud (Fig. 5) show that the mushroom cloud developed very rapidly, with an initial radial velocity between 15:40 and 15:45 of 55 m/s. The cloud had expanded 15 km upwind of the western edge of the zone of devastation by 15:50, at which time the cloud reached a stagnation point upwind, but continued to grow in downwind and crosswind directions. The relationships at the stagnation point are remarkably simple. The upwind stagnation point represents the distance at which there was a balance between the radial expansion velocity and the local wind velocity. NOAA satellite

data (Sarna-Wojcicki et al., 1981) show that the feather-edge of the cloud extended between 12 and 16 km altitude. The wind velocities at Spokane (Washington) recorded by the U.S. National meteorological service at these altitudes on May 18 varied between 12 and 33 m/s, averaging 22 m/s. Between 15:50 and 16:10 the horizontal radial expansion velocity of the cloud was fairly steady, between 25 and 20 m/s. For the next hour the western edge moved eastwards at about 5 m/s, as the eruption weakened.

One effect of the wind on the cloud is to gradually push the center of symmetry of the cloud downwind. Figure 6 shows the distance, at each successive time, of the center from the cross marked on Fig. 5. The cross is assumed to represent the center of symmetry at 15:37.5, when cloud ascent initiated. After 15:45 the center of symmetry is moved downwind at a fairly constant velocity of 14.8 m/s. This velocity is approximately half of the observed stratospheric wind speed. The easternmost (downwind) edge of cloud reached a steady velocity of 30 m/s after 15:50 GMT; this cloud edge is thought to be purely wind-driven, corresponding to the maximum stratospheric velocity observed at 10 to 12 km on May 18.

Wind direction information measured at Spokane at 17:20 GMT is shown in Fig. 5 at elevations of 5, 8, and 20 km. Initially the outer edge of the cloud (at 15:45, for example) is elongated ENE under the influence of the low-level winds, but at later times is elongated E to ESE as the winds at higher altitude influence the cloud's shape.

A prominent feature of the mushroom cloud can be noted in cross-sections of the cloud seen via radar observations (Sarna-Wojcicki et al., 1982). Although the cloud immediately above the source region reached 25 to 30 km, the altitude of the upper surface decreases radially away to about 20 km. This behavior is typical of a plume intruded into a stratified environment (Turner, 1979). The momentum of the cloud takes dense material to a height where it is now surrounded by lower-density air. The material then flows outwards and downwards to its own density level. Higher-altitude winds were also relatively light.

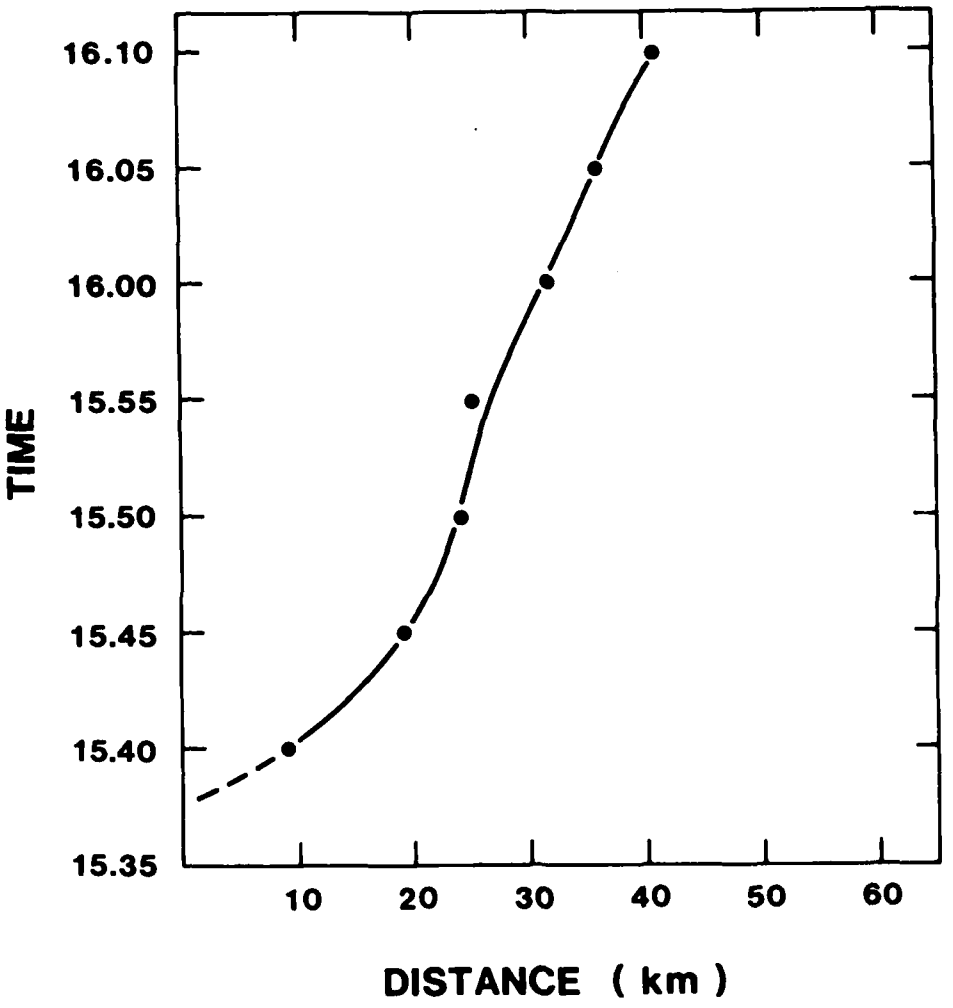

Fig. 6. Distance in km of the center of symmetry of the radially expanded cloud from the cross marked in Fig. 5.

Figure 1 shows that the ascending column beneath the umbrella region converges inwards. Eruption columns originating from a localized vent expand with height as the ascending plume entrains air. Such columns can be approximately treated as if they emerge from a point source. The giant cloud, however, originated from a large area. Turner (1979) has discussed how inward flow is typical of buoyancy generated from a heated surface, because a thermal boundary layer is created. The fluid streamlines in this boundary flow converge into an ascending region that is narrow compared to the width of the source area. The effect is evidently dominating the effect of entrainment in the Mount St. Helens cloud because of the large area providing the source of buoyancy.

Finally, we note that the mosaic photographs (Fig. 1) show a prominent concentric ring structure in the lower part of the cloud and prominent radial protrusions in the uppermost outwardly expanding parts of the cloud. The radial protrusions have also been observed in the eruption cloud of Hekla in 1947 (Thorarinsson, 1970). We are not yet clear about the significance of these structures.

III. THE DEPOSITS

The deposits formed from the blast and the eruption cloud (Clouds III and IV) have been extensively studied (Moore and Sissons, 1981; Waitt, 1981; Waitt and Dzurisin, 1981; Hobblitt et al., 1981; Walker and McBroome, 1983). This work allows estimates to be made of the volumes of material in the cloud and the initial temperature of the pyroclastic mixture.

The surge and flow facies of the blast deposit have an estimated volume of 0.18 km^3 (Moore and Sisson, 1981; Moore and Rice, 1984) or 0.1 km^3 (D.R.E.). The associated air-fall deposit has a volume of 0.06 km^3 (0.03 km^3 D.R.E.) within 90 km of the volcano, as deduced from the isopach map of unit A3 (Fig. 7) together with data presented by Waitt and Dzurisin (1981). This is probably an underestimate, as a significant proportion of the fine ejecta injected to altitudes of 20 km or more would be blown hundreds of kilometers downwind. In Fig. 7 we draw attention to the observation that the isopach map of A3 covers an area whose width in the crosswind direction is approximately that of the giant cloud. The maximum thickness of 6 cm does not coincide with the volcanic vent of Mount St. Helens, but occurs in an area about 12 km to the north of the volcano. This can be compared with the isopach map of the plinian airfall deposit, which shows the point source vent rather than the broad zone of A3 (Fig. 5b). We also note that the A3 deposit is often rich in accretionary lapilli, which comprise up to 50% of the entire deposit. In addition to typical accretionary lapilli, clusters of ash grains occur at scales smaller than those normally considered as accretionary lapilli. Liquid water, therefore, probably comprised at least 10% by weight of the deposit.

The blast deposit consists of about 50% poorly vesicular juvenile dacite blocks and assorted lithic material of the old volcanic structure. Moore and Sissons (1981) estimate initial temperatures of at least 350°C for this mixture, based on the extent of charring of the timber. This is consistent with an equal mix of cold lithics and juvenile dacite clasts (at 850°C) which would have a mean temperature of about 400°C. Hoblitt et al. (1981) measured temperatures up to 277°C in the thickest pyroclastic flow deposits, but

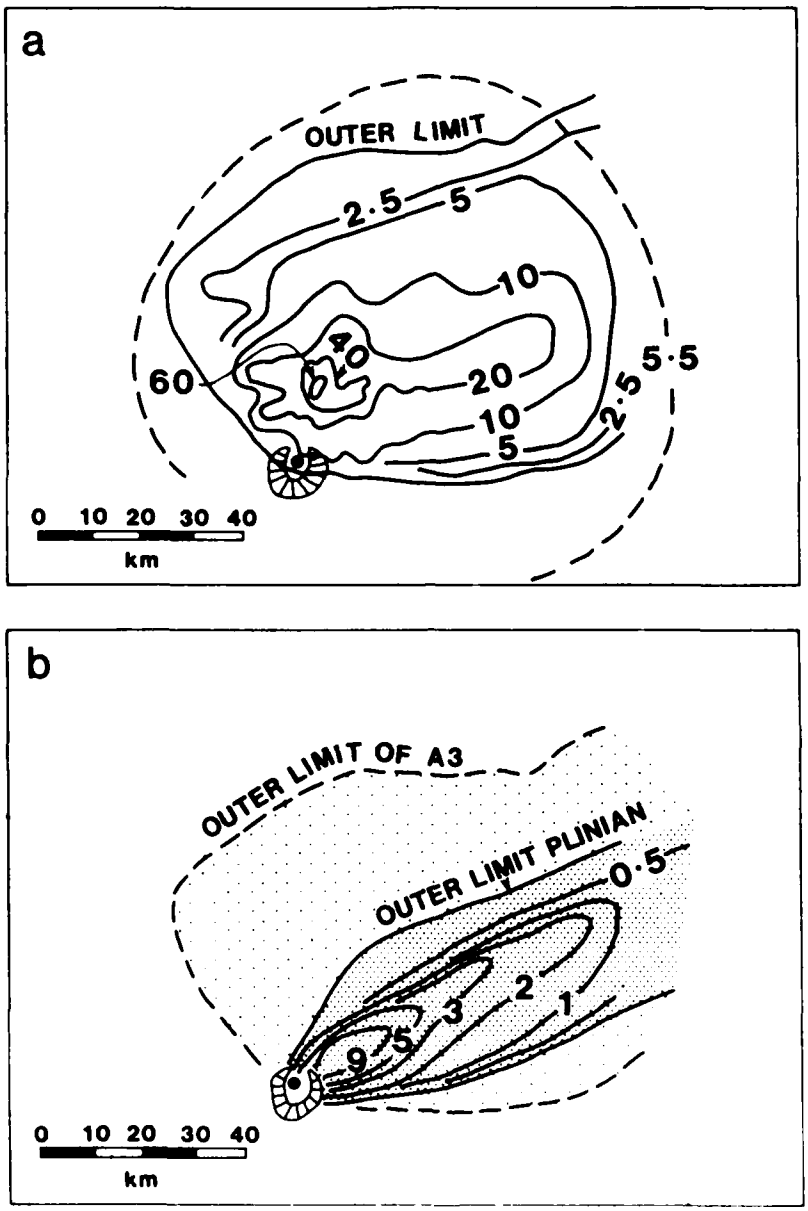

Fig. 7. (a) Isopach map of the air-fall deposit from the giant cloud, simplified from Sisson (1982). Contours are in millimeters. The dashed line shows the outline of the giant cloud at 15.55 GMT. (b) Isopach map of proximal plinian deposit, after Waitt (1981), showing relationship to point-source vent. The outer limit of the giant ash cloud is shown for comparison.

generally found temperatures below 160°C. Much of the ejecta, occurring as thin layers mantling topography, can be assumed to have been emplaced at even lower temperatures. Some of the temperature decrease observed can be attributed to the decompression of the flow mixture during transport (Kieffer, 1981). Conversion of initial heat and energy stored in compression in the gases into kinetic energy resulted in the high flow velocities, and some cooling of the flow. Some of the heat was also transferred to the atmosphere during emplacement as the flow mixed with its surroundings, and this thermal energy source provides the main cause of cloud ascent.

Walker and McBroome (1983) have drawn attention to the fines-depleted character of the blast deposits. In particular the basal coarse-grained layer A1 is strongly fines-depleted, and they argue that the ash-fall deposit A3 represents the complementary lost fines. The layer A2 deposit is also poorer in fines than most flow deposits. Irrespective of the relative merits of the flow and surge views, the grain-size data indicate extensive mixing of air with the solid ejecta, creating fines-depleted flow (surge?) deposits and fines-enriched ash-fall deposits.

IV. THEORETICAL CONSIDERATIONS

The observations in the preceding section suggest that the formation of the main cloud was an abrupt event at the end of blast emplacement. This is interpreted as a consequence of the flow becoming lighter than the overlying air. Three main processes that caused the flow to decrease in density as it moved away from the source can be identified: decompression of the blast mixture of solids and gas, mixing and heating of the surrounding air into the flow, and sedimentation from the flow.

There is general agreement that the blast was triggered by the landslide, which cause a major pressure drop within the volcano. Photographic evidence indicates that about 500 m of rock overburden was removed (Kieffer, 1981; Eichelberger and Hayes, 1982). However, there are two different models for the explosions that supplied the blast flow. In the hydrothermal model the reservoir is assumed to be a mixture of water and rock at or below the saturation temperature and pressure. In this case the initial pressure may be considered to be between the lithostatic pressure of 500 m of overburden (approximately 125 bars) and the hydrostatic pressure of the hydrothermal fluid, which might be considerably lower. In the magmatic model the reservoir is assumed to be high-temperature magma containing a small fraction of exsolved water (Eichelberger and Hayes, 1982). The amount of cooling of the mixture and the change in bulk density due to decompression are quite sensitive to the initial conditions and model assumed. Unfortunately both models give plausible explanations of the observed high velocities of the blast flow.

Hydrothermal models require mass fractions of water in the reservoir of at least 0.02 to over 0.1 to achieve the observed velocities of 100 to 150 m/s. They also result in substantial cooling of the blast flow mixture during decompression because of the heat of vaporization and the large mass fraction of water. For example, in the model of Kieffer (1981) the mixture cools from 327°C to 225°C in decompressing from 125 bars to atmospheric pressure. Kieffer argued that the flow could become underpressured in some regions and therefore the cooling would be even greater. Her calculations suggest that

underpressured regions could approach the density of the overlying atmosphere and that this could cause the flow to become buoyant. In the calculations presented by Kieffer (1981) the flow density approaches 2 kg/m^3 in distal regions, compared to an overlying atmosphere with a density of about 0.8 kg/m^3.

In the magmatic model the mass fractions of gas required to account for the observed velocities are much smaller and are estimated to be less than 0.006 by Eichelberger and Hayes (1982). As the water vapor is initially at high magmatic temperatures, there is no heat of vaporization as an energy sink, so that the cooling on expansion is much less than in the hydrothermal model. For example, a mass fraction of water equal to 0.006 would only cause a temperature decrease of the bulk solid/gas mixture of about 13°C during expansion from 125 bars to atmospheric pressure. The main cause of a decrease in temperature in this model is the incorporation of cold lithic clasts during the explosion, which could have resulted in a temperature decrease of 400 to 450°C from the magmatic values (850°C to 900°C). A feature of a magmatic model is that the density of the solid and gas mixture is still high when decompressed to one atmosphere, because of the small mass fraction of gas. For example, at 450°C and a water content of 0.006 the mixture would have a bulk density of 42 kg/m^3.

Geological evidence does not favor a purely hydrothermal model, as argued in detail by Eichelberger and Hayes (1982). About half the ejecta is juvenile vesicular dacite and some of the temperatures inferred for the flow appear too high for a shallow hydrothermal system. An important magmatic component to the explosion is indicated. We conclude that decompression by itself could not have caused the flow to have become buoyant and cannot account for the coolings observed during flow. Nevertheless, a significant contribution of hydrothermal fluids to the explosion cannot be discounted, and the role of decompression in reducing the flow density remains a major uncertainty.

A second process by which the blast flow would reduce its density would be by mixing and heating of surrounding air as the flow advanced over the rough topography around Mount St. Helens. The complicated and pressurized

character of the flow (Kieffer, 1981) and the irregularity of the ground makes impossible a theoretical assessment of how much entrained air would be expected. As an alternative we calculate how much air would need to be incorporated into the flow to reduce the density to that of the atmosphere. We make the assumption that the mixture is homogeneous, while recognizing that the real flow is much more complex. The idea of the calculations is to assess the average proportions of air required to make the flow buoyant. The conditions for this to happen can be approximately estimated by considering the heat balance between the pyroclasts and the air and the definition of the bulk density, which are given respectively by the following expressions:

$$c_m M_m(\theta_e - \theta_c) = c_a M_a(\theta_c - \theta_a) \tag{1}$$

and

$$\alpha/\beta_c = \frac{\theta_c(1 - n_c)}{\theta_a} + n_c \frac{\alpha}{\sigma} \tag{2}$$

where c_m and c_a are the specific heat capacities of pyroclasts (m) and air (a), M_m and M_a are the total masses of pyroclasts and air in the mixture, θ_e is the pyroclast temperature, θ_a is the ambient air temperature, θ_c is the mixture temperature, α is the ambient air density, β_c is the bulk mixture density, n_c is the mass fraction of solids, and σ is the pyroclast density. With the following definitions,

$$n_c = \frac{\bar{M}}{1 + \bar{M}} \tag{3a}$$

and

$$\bar{M} = \frac{M_m}{M_a} \tag{3b}$$

Eqs. (1) and (2) can be considered to give

$$\frac{\alpha}{\beta_c} = \frac{(c_m \bar{M} \theta_e + c_a \theta_a)}{(c_a + \bar{M} c_m)(1 + \bar{M}) \theta_a} + \left(\frac{\bar{M}}{1 - \bar{M}}\right) \frac{\alpha}{\sigma} \tag{4}$$

Appropriate choices of the various parameters are listed in Table 1. The values of air temperature and density are estimated by using data recorded at a meteorological station in eastern Washington on May 18, 1980. The air temperature varied from -3°C to -23°C and the air density from 0.83 to 0.61 kg/m^3 over the height interval 2.5 to 4 km above sea level. The height interval corresponds to that where mixing occurred between the blast flow and the atmosphere. The critical condition for convective lift-off is that α/β_c = 1.0. If the total mass of ejecta is included in the calculation (M_m = 3.25×10^{11} kg), the mass of air at α/β_c = 1.0 is 5.0×10^{11} kg (625 km^3 at a density of 0.7 kg/m^3) and the mean mixture temperature is 152°C. Over the 600-km^2 area of the blast, this mass of air is approximately equivalent to a layer of air 1200 m thick. These are maximum values since it is likely that the flow became buoyant not only by heating air but by sedimentation. The amount of air required will also decrease as the amount of hydrothermal fluid involved in the mixture increases, since the effect of adding steam is to reduce flow density further.

A minimum estimate can be obtained if only the mass of ejecta in the air fall deposit is used ($M_m = 0.75 \times 10^{11}$ kg). The calculated temperature estimate remains the same, but the air mass decreases to 10^{11} kg, equivalent to a layer thickness of 250 m. This calculation is probably too low, since we suspect the volume estimate of A3 is conservative. Varying the input parameters by amounts consistent with observations (Table 1) would not change these results significantly. The blast flow has to mix with enough air and sediment enough coarse ejecta to form a flow several hundred meters thick, to allow the density to fall sufficiently to form the major convective cloud.

The blast flow moved across the surface, progressively mixing with air. We propose that the flow terminated when a critical mass of air had been engulfed and a critical mass of sediment had been deposited. The blast flow became buoyant and lifted off to form the giant cloud. The calculations are broadly consistent with observations. The visible depth of the flow was about 1 km (Moore and Rice, 1984) and the temperatures of the deposits were mostly less than 160°C, suggesting that more than half the thermal energy had been transferred to admixed air.

Table 1. Values of Physical Parameters Used in Calculations on Cloud Formation

$M_m = 3.25 \times 10^{11}$ kg
$\alpha = 0.8$ kg/m^3
$\theta_e = 400°C$
$\theta_a = 0°C$
$\sigma = 2500$ kg/m^3
$c_a = 993$ J kg^{-1} K^{-1}
$c_m = 1100$ J kg^{-1} K^{-1}

Thus we assume that when the cloud became buoyant it had a temperature of 150°C, carried a mass of particles equivalent to that which formed the air-fall layer of 7.5×10^{10} kg, and had a mass of air of 5.0×10^{11} kg. The total thermal energy of this material is 1.07×10^{17} joules, and the density at an altitude of 3 km (air density and temperature 0.7 kg/m^3 and -10°C, respectively) is 0.48 kg/m^3. Using these estimates for the conditions of the rising cloud, we can compare the observed altitude and ascent rate with theoretical relationships for gravitational convection.

Morton et al. (1956) considered the instantaneous release of a source of buoyancy. For the case of a thermal they estimate that the final height H is a function of the total thermal energy, Q:

$$H = KQ^{1/4} \tag{5}$$

This relationship was derived by considering the buoyant rise in a stably stratified atmosphere, and the constant K is a parameter depending on the environmental temperature gradient and lapse rate. For a standard atmosphere, K = 1.4. Strictly this formulation should not be valid for columns much higher than the stratosphere. However, Sparks (1986) has carried out numerical calculations on plume ascent which do not strongly depart from predictions based on Morton et al.'s treatment of gravitational convection, even for heights of 30 km. For $Q = 1.07 \times 10^{17}$ joules, H is 25.3 km, which is in remarkably good agreement with the height reached by Cloud III (Fig. 1).

If the cloud is regarded as a maintained plume of short duration at 25 km, column calculations (Sparks, 1986) indicate a power input of 2.0×10^{14} joules/sec lasting over a 9-min period. This is also consistent with observations, since the major period of cloud growth lasted 10 min.

The ascent profile for Cloud III can also be interpreted in terms of a simple physical model. Wilson and Self (1980) analyzed the ascent of some small eruption clouds from the volcano Fuego in Guatemala in terms of the ascent of a buoyant cylinder of length L. They equated the product of mass and acceleration to the total forces acting on the cloud (atmospheric drag, gravity, and buoyancy) to derive the following expression:

$$\frac{\beta_c}{\alpha} = \frac{g - (C_d\, u^2/2L)}{g + du/dt} \qquad (6)$$

where C_d is the drag coefficient, u is the velocity of the cloud front, L is taken as the cloud height, g is the acceleration due to gravity, and du/dt is the acceleration of the cloud. We have used this relationship to estimate the relative density β_c/α. The results are listed in Table 2 for C_d = 1.00 up to 18 km high. Above 18 km the cloud has expanded so much that the analysis is unlikely to be valid. The most significant feature of the calculations is that the cloud is still buoyant at 8 km altitude, but has become denser than the surrounding atmosphere by 13.3 km. The level of neutral density (β_c/α = 1.0) is about 10 km high. This agrees well with radar data (Sarna-Wojcicki et al., 1981) that show that the base of the mushroom cloud was at 10 km, confirming that the cloud had reached its neutral-density level at this height.

The ascent of the cloud to 25 km high is entirely due to the column's inertia. The cross-section of the column shows a bulge at the top as the cloud overshoots to 25 km due to momentum and then flows radially outwards and slightly downwards to form a forced intrusion between 10 and 20 km altitude. The anvil shape of the mushroom is characteristic of experimental force intrusions formed by the ascent of buoyant plumes into a stratified environment (Turner, 1979).

The radial expansion of the cloud can be explained by continuity considerations. The mean radial velocity, V_R, can be approximately related to the total mass flux of air and pyroclasts at the base of the mushroom cloud (at 10 km high), where the ascending material has the same density, α_a, as the surrounding atmosphere, by the following expression:

$$V_R = \frac{\alpha_a\, u\, A}{\bar{\alpha}\, 2\, \pi\, HR} \qquad (7)$$

where R is the radial distance, A is the cross-sectional area of the ascending cloud, u is its velocity, $\bar{\alpha}$ is the mean air density between the top and base of the mushroom cloud (10 to 20 km in this case), and H is the thickness of

Table 2. Values of Parameters Used in Calculations with Eq. (6)

h (km)	L (km)*	u (m/s)	du/dt (m/s^2)	β/α
8	6	111	0	0.895
13.3	11.3	78	-0.50	1.024
18.0	16.0	37.5	-0.33	1.030

*Note that the value of L is the height minus altitude of the ground above sea level (2 km).

the mushroom cloud. A value of A equal to 500 km^2 rather than the 600 km^2 of the blast area is estimated, since the cloud's cross-sectional area decreases in height up to the height of neutral density at 10 km. Taking values of $\bar{\alpha}$ = 0.2 kg/m^3, α_a = 0.41 kg/m^3, u = 80 m/s, H = 10 km, and A = 500 km^2, Eq. (7) simplifies to

$$V_R = \frac{1.3 \times 10^6}{R} \tag{8}$$

Figure 8 compares this simple relationship with the data of radial velocity versus distance, calculated by taking the average velocity between each 5-min contour in Fig. 5. Although the intrusion of the mushroom cloud into the atmosphere is likely to involve mixing, the simple analysis appears to be sufficient to model the gross features of the formation of the umbrella-shaped cap.

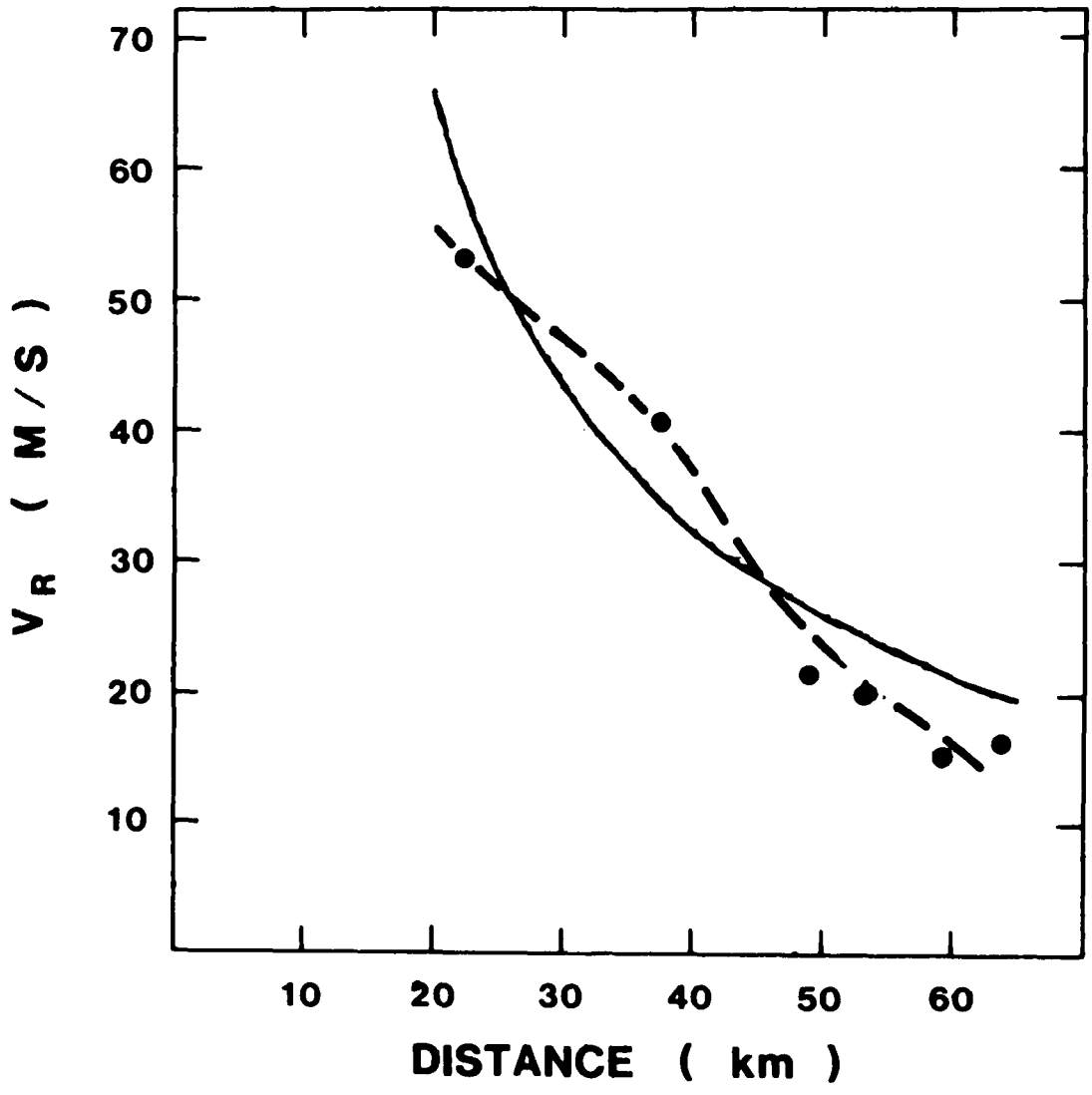

Fig. 8. Radial expansion velocity of mushroom cloud versus cloud diameter. Line represents prediction of simple theory [see Eq. (7)].

V. DISCUSSION

Large eruption columns have usually been associated with vertical explosions arising directly from volcanic vents. The initial events of May 18, however, have revealed a quite different mechanism involving the spread of an energetic blast flow. The flow eventually mixed with enough air to provide a source of buoyant hot air and ash over a 600-km^2 area. The transition from horizontal density flow to convective ascent was abrupt, lasting only 1.5 min.

There are several features that distinguish eruption clouds formed in this way. First, the center of cloud ascent can be displaced away from the volcano, by 12 to 13 km in this case (Figs. 5 and 7). The source of buoyant air and ash is a large area rather than a point source, and consequently the thickness of the air-fall deposit should be uniform in proximal areas, with closure around the center of the blast rather than around the volcano. This feature is observed with the air-fall deposit of the Mount St. Helens cloud (Fig. 7a). There is no momentum-dominated basal region to the column, as is the case for eruption columns generated by explosions (Sparks and Wilson, 1976). The cloud is only formed when the flow material becomes buoyant, and must involve an initial stage of acceleration, rather than deceleration as in explosion-generated clouds. The Mount St. Helens cloud only entrained fine-grained material: Hoblitt et al. (1981) and Walker and McBroome (1983) report only fine-grained ash less than 2 mm in diameter within the deposit. Coarse pyroclasts were segregated into the flow deposit. The vertical velocities of 110 m/s at 8 km are sufficient to carry fragments of 10 cm diameter or more, but the air-fall deposit only contains fine-grained ash less than 0.2 in diameter. This observation indicates that the coarse ground material is segregated at low altitudes, well below 8 km where the maximum velocity is observed.

Sparks and Walker (1977) have proposed that pyroclastic flows are associated with the formation of voluminous air-fall deposits as well as ignimbrite. Three sources of fine ash for these deposits were proposed: (1) the escape of fine ash and gas above the collapsing eruption column; (2) the

escape of fine ash as a dense flow segregates near the vent; and (3) the elutriation of fine ash from the moving fluidized flow. The behavior of the May 18 flow suggests the possibility that a substantial part of co-ignimbrite ash clouds can be formed abruptly over the whole area of the ignimbrite during the final stages of emplacement. The fine grain size and wide distribution of co-ignimbrite ash layers are more consistent with this mechanism.

The dramatic expansion of the mushroom cloud is of general significance. The reason for the upwind flow and large radial velocities is the large total volume flux of air and ash from the vertical plume that supplies the cloud. The volume flux is in turn related to the temperature and mass flux of solids (Wilson et al., 1978; Sparks, 1986). Irrespective of whether the cloud is fed from a point source (as in plinian eruptions) or from a large area (as in the present case), the development of a large umbrella cloud should also be a feature of all eruption columns supplied by large mass fluxes. Sparks (1986) has calculated that plinian eruption columns with heights greater than 20 km and mass eruption rates greater than 5×10^4 m^3/s should show large mushroom clouds and significant upwind flow.

The development of large radial flow velocities over large horizontal distances has major implications for the dispersal and grain-size characteristics of air-fall deposits. Carey and Sparks (1986) have calculated the trajectories of clasts through eruption columns that have large enough mass-discharge rates to form a mushroom cloud. The distribution of maximum fragment size is strongly influenced by transport within the horizontally expanding mushroom cloud. The areas enclosed by maximum-grain-size isopleths are not influenced by either the wind or the ascent in the plume. Maximum-grain-size data are controlled by the dimensions and velocities of the mushroom cloud. Hence the column height and mass discharge rate can be estimated quite accurately from maximum-grain-size maps.

REFERENCES

Carey, S. N. and Sparks, R. S. J., 1986. Quantitative models of the fall-out and dispersal of tephra from volcanic eruption columns. Bulletin of Volcanology (subjudice).

Eichelberger, J. C. and Hayes, D. B., 1982. Magmatic model for the Mount St. Helens blast of May 18, 1980. J. Geophys. Res. 87: 7727-7738.

Hoblitt, R. P. and Miller, C. D., 1984. Comments and reply on "Mount St. Helens 1980 and Mont Pelee 1902 - Flow or Surge?" Geology 12: 692-693.

Hoblitt, R. P., Miller, C. D. and Vallance, J. W., 1981. Origin and stratigraphy of the deposit produced by the May 18th directed blast. U.S. Geological Survey Prof. Paper 1250: 401-420.

Kieffer, S. W., 1981. Fluid dynamics of the May 18th blast at Mount St. Helens. U.S. Geological Survey Prof. Paper 1250: 379-400.

Moore, J. G. and Rice, C. J., 1984. Chronology and character of the May 18, 1980, explosive eruptions of Mount St. Helens. National Academy of Sciences, Special Volume on Volcanic Eruptions: 133-142.

Moore, J. G. and Sisson, T. W., 1981 Deposits and effects of the May 18 pyroclastic surge. U.S. Geological Survey Prof. Paper 1250: 421-438.

Morton, B. R., Taylor, G. I. and Turner, J. S., 1956. Turbulent gravitational convection from maintained and instantaneous sources. Proc. Roy. Soc. A234: 1-23.

Rice, C. J., 1981. Satellite observations of the Mount St. Helens eruption of 18 May 1980. Proc. of S.P.I.E. (International Society for Optical Engineering) 278: 23-31.

Sarna-Wojcicki, A. M., Shipley, S., Waitt, R. B., Dzurisin, D. and Wood, S. Y., 1981. A real distribution, thickness, mass, volume and grain size of air-fall ash from the six major eruptions of 1980. U.S. Geological Survey Prof. Paper 1250: 577-600.

Sisson, T. W., 1982. Sedimentary characteristics of the air-fall deposits produced by the major pyroclastic surge of May 18, 1980 at Mount St. Helens, Washington. Master's Thesis, University of California at Santa Barbara, 145 pp.

Sparks, R. S. J., 1986. The dimensions and dynamics of volcanic eruption columns. Bulletin of Volcanology (subjudice).

Sparks, R. S. J. and Walker, G. P. L., 1977. The significance of vitric-enriched air-fall ashes associated with crystal-enriched ignimbrites. J. Volcanol. Geotherm. Res. 2: 329-341.

Sparks, R. S. J. and Wilson, L., 1976. A model for the formation of ignimbrite by gravitational column collapse. J. Geol. Soc. Lond. 132: 441-451.

Thorarinsson, S., 1970. Hekla, a notorious volcano. Almenna Bokafelagid, Reykavik.

Turner, J. S., 1979. Buoyancy effects in fluids. Cambridge University Press.

Waitt, R. B., Jr., 1981. Devastating pyroclastic density flow and attendant air fall of May 18 - stratigraphy and sedimentology of deposits. U.S. Geological Survey Prof. Paper 1250: 439-458.

Waitt, R. B., Jr., 1984. Comments and reply on "Mount St. Helens 1980 and Mont Pelee 1902 - Flow or Surge?" Geology 12: 693.

Waitt, R. B. and Dzurisin, D., 1981. Proximal air-fall deposits from the May 18 eruption: stratigraphy and field sedimentology. U.S. Geological Survey Prof. Paper 1250: 601-616.

Walker, G. P. L. and McBroome, L. A., 1983. Mount St. Helens 1980 and Mount Pelee 1902 - Flow or Surge? Geology 12: 571-574.

Walker, G. P. L. and McBroome, L. A., 1984. Comments and reply on "Mount St. Helens 1980 and Mount Pelee 1902 - Flow or Surge?" Geology 12: 693-695.

Wilson, L. and Self, S., 1980. Volcanic explosion clouds: density, temperature, and particle content estimates from cloud motion. J. Geophys. Res. 85: 2567-2572.

Wilson, L., Sparks, R. S. J., Huang, T. C. and Watkins, N. D., 1978. The control of volcanic column heights by eruption energetics and dynamics. J. Geophys. Res. 83: 1829-1836.

U. S. Forest Service, Pacific Northwest Region, 1981. Mount St. Helens Land Management Plan, Final Environmental Impact Statement: Vancouver, Washington, U.S. Forest Service, 162 pp.

LABORATORY OPERATIONS

The Aerospace Corporation functions as an "architect-engineer" for national security projects, specializing in advanced military space systems. Providing research support, the corporation's Laboratory Operations conducts experimental and theoretical investigations that focus on the application of scientific and technical advances to such systems. Vital to the success of these investigations is the technical staff's wide-ranging expertise and its ability to stay current with new developments. This expertise is enhanced by a research program aimed at dealing with the many problems associated with rapidly evolving space systems. Contributing their capabilities to the research effort are these individual laboratories:

Aerophysics Laboratory: Launch vehicle and reentry fluid mechanics, heat transfer and flight dynamics; chemical and electric propulsion, propellant chemistry, chemical dynamics, environmental chemistry, trace detection; spacecraft structural mechanics, contamination, thermal and structural control; high temperature thermomechanics, gas kinetics and radiation; cw and pulsed chemical and excimer laser development including chemical kinetics, spectroscopy, optical resonators, beam control, atmospheric propagation, laser effects and countermeasures.

Chemistry and Physics Laboratory: Atmospheric chemical reactions, atmospheric optics, light scattering, state-specific chemical reactions and radiative signatures of missile plumes, sensor out-of-field-of-view rejection, applied laser spectroscopy, laser chemistry, laser optoelectronics, solar cell physics, battery electrochemistry, space vacuum and radiation effects on materials, lubrication and surface phenomena, thermionic emission, photosensitive materials and detectors, atomic frequency standards, and environmental chemistry.

Computer Science Laboratory: Program verification, program translation, performance-sensitive system design, distributed architectures for spaceborne computers, fault-tolerant computer systems, artificial intelligence, microelectronics applications, communication protocols, and computer security.

Electronics Research Laboratory: Microelectronics, solid-state device physics, compound semiconductors, radiation hardening; electro-optics, quantum electronics, solid-state lasers, optical propagation and communications; microwave semiconductor devices, microwave/millimeter wave measurements, diagnostics and radiometry, microwave/millimeter wave thermionic devices; atomic time and frequency standards; antennas, rf systems, electromagnetic propagation phenomena, space communication systems.

Materials Sciences Laboratory: Development of new materials: metals, alloys, ceramics, polymers and their composites, and new forms of carbon; nondestructive evaluation, component failure analysis and reliability; fracture mechanics and stress corrosion; analysis and evaluation of materials at cryogenic and elevated temperatures as well as in space and enemy-induced environments.

Space Sciences Laboratory: Magnetospheric, auroral and cosmic ray physics, wave-particle interactions, magnetospheric plasma waves; atmospheric and ionospheric physics, density and composition of the upper atmosphere, remote sensing using atmospheric radiation; solar physics, infrared astronomy, infrared signature analysis; effects of solar activity, magnetic storms and nuclear explosions on the earth's atmosphere, ionosphere and magnetosphere; effects of electromagnetic and particulate radiations on space systems; space instrumentation.

...

END

2-87

DTIC